A new class of OLD family ATPases functions in cell cycle progression in thermoacidophilic archaea

Yunfeng Yang[1], Shikuan Liang[1], Junfeng Liu[1], Xiaofei Fu[1], Pengju Wu[1], Haodun Li[1], Jinfeng Ni[1], Qunxin She[1], Mart Krupovic[2], Yulong Shen[1]*

[1]CRISPR and Archaea Biology Research Center, State Key Laboratory of Microbial Technology, Microbial Technology Institute, Shandong University, 266237, Qingdao, China

[2]Institut Pasteur, Université Paris Cité, CNRS UMR6047, Archaeal Virology Unit, Paris, France

*Correspondence: yulgshen@sdu.edu.cn

ABSTRACT

Overcoming lysogenization defect (OLD) proteins are diverse ATPases-nucleases functioning in antiphage defense in bacteria. However, the role of these proteins in archaea is currently unknown. Here, we describe a new class of archaeal OLD family ATPases and show that they are not involved in antiviral defense but play an essential role in cell cycle progression. We show that an OLD family enzyme of *Saccharolobus islandicus* REY15A (SisOLD) is essential for cell viability and exhibits cyclic expression patterns at both transcriptional and translational levels, displaying the peak expression during the genome synthesis (S) cell cycle phase. SisOLD overexpression or knockdown leads to significant growth retardation, cell size enlargement, and increased cellular DNA content. We demonstrate that the ATPase activity but not the nickase activity of SisOLD is crucial for the normal cell cycle progression. Notably, SisOLD copurifies with chromatin-associated proteins, such as Cren7 and a histone deacetylase homolog, suggesting involvement in chromosome remodeling following its replication. Collectively our results suggest that SisOLD plays an important role in chromatin processing and remodeling, revealing a novel function of OLD family proteins.

KEY WORDS

Archaea, *Saccharolobus islandicus*, OLD family protein, ATPase, nickase, cell cycle

INTRODUCTION

Overcoming lysogenization defect (OLD) family proteins are ATP-powered nucleases that are widely distributed in bacteria, archaea, phages, and plasmids (1). Recent bioinformatic, genetic, and structural studies have clarified the functioning and evolution of this protein family (2-4). These enzymes contain an N-terminal ATPase domain of the ATP-binding cassette (ABC) superfamily and a C-terminal TOPRIM (Topoisomerase-primase) domain nuclease (5). OLD family proteins have been classified into four classes based on gene neighborhood, biochemical properties, domain organization, and catalytic mechanisms (1). Class 1 OLD family enzymes are encoded by standalone genes within variable gene neighborhoods and have been implicated in various virus-host and virus-virus antagonistic interactions. Indeed, the founding member of the family has been discovered in bacteriophage P2, with genetic studies showing that the *old*-bearing phage P2 kills *Escherichia coli recB* and *recC* deficient hosts upon infection and specifically interferes with phage λ replication (6). By contrast, class 2 OLD ATPases-nucleases are always encoded in tandem with UvrD/PcrA/Rep-like helicases (7), with the two enzymes, denoted GajA and GajB, respectively, constituting the recently described 'Gabija' antiviral defense system (1,2). Class 3 OLD ATPases-nucleases are commonly found in retrons, another defense system centered around a reverse transcriptase (*ret*) gene and a non-coding RNA (8-10). Class 4 OLD enzymes constitute the PARIS defense system, with the ATPase and TOPRIM catalytic domains being encoded separately by adjacent genes, denoted *ariA* and *ariB* (11). Although the properties of the OLD family enzymes have been explored extensively, focusing on the abortive infection of P2 lysogens in the 1970s (7,12-14) and, recently, on the mechanisms of several defense systems (3,4,15), it remains unclear whether the OLD family enzymes have any non-antiviral functions *in vivo*. To the best

of our knowledge, none of the archaeal OLD ATPases-nucleases has been characterized and reported.

Archaea are divided into four phyla or superphyla, namely, Euryarchaeota, TACK superphylum, Asgardarchaeota, and DPANN superphylum (16,17). In addition to sharing common origin of information processing machineries with Eukarya, archaea of the Asgardarchaeota and TACK superphylum encode many proteins that were initially thought to be specific of eukaryotes (17,18). In particular, species of the order Sulfolobales from the TACK superphylum have a cell cycle resembling that of eukaryotes (19,20), including G1 (Gap 1), S (DNA synthesis), G2 (Gap 2), M (chromosome segregation), and D (cell division) phases (21). The cell division machinery of Sulfolobales consists of archaea-specific protein CdvA, four eukaryotic ESCRT-III homologs, namely, ESCRT-III (also known as CdvB), ESCRT-III-1 (CdvB1), ESCRT-III-2 (CdvB2), and ESCRT-III-3 (CdvB3), and the AAA^+ ATPase Vps4 homolog (CdvC) (22-25). Although the role of ESCRT machinery in the Sulfolobales cytokinesis has been firmly established, the regulation of the cell cycle progression remains unclear. The expression of the *cdvA* is transcriptionally controlled by a repressor aCcr1 (26,27), whereas the subsequent degradation of CdvB by the proteasome is reported to control the cytokinesis progression (23). However, the regulation of the other cell cycle phases, especially G1 and S, is unknown. Because Eukarya is believed to originate from archaea, elucidating the cell cycle regulation in archaea could provide insights into the origin and evolution of the eukaryotic cell cycle regulation mechanisms.

In this study, we characterize an OLD family protein from *S. islandicus* REY15A (order Sulfolobales), one of the few genetically tractable representatives of the TACK superphylum. We show that the gene coding for SisOLD is conserved across Sulfolobales and is essential for the cell viability. Unexpectedly, this protein does not appear to participate in antivirus defense but instead is involved in cell cycle progression, with its ATPase activity, but not the nuclease activity, being critical for this

function. Our study expands the understanding on the functional versatility of the OLD family proteins and provides insight into the cell cycle regulation in Sulfolobales.

MATERIALS AND METHODS

Strains and growth conditions

Saccharolobus islandicus E233S(Δ*pyrEF*Δ*lacS*) (Supplementary Table S1) was grown in STVU medium containing mineral salt, 0.2% (w/v) sucrose (S), 0.2% (w/v) tryptone (T), 0.01% (w/v) uracil (U) and a mixed vitamin solution (V). The medium was adjusted to pH 3.3 with sulfuric acid, as described previously (28). STV medium containing 0.2% (w/v) tryptone (T) was used for screening and cultivating uracil prototrophic transformants. ATV medium containing 0.2% (w/v) D-arabinose(A) was used for protein expression. Culture plates were prepared using gelrite (0.8% [w/v]) by mixing 1 × STV and an equal volume of 1.6% gelrite. Plasmid cloning and protein expression were performed with *E. coli* DH5α and BL21 (DE3)-RIL, respectively. The cells were cultured in Lysogeny-Broth (LB) medium supplemented with appropriate antibiotics. Plaque assay was performed using *E. coli* MG1655. The strains constructed and used in this study are listed in the Supplementary information (Supplementary Table S1).

Construction of plasmids

Construction of SisOLD knockout and *in situ* gene tagging of *sisOLD* strains was according to the endogenous CRISPR-Cas-based genome editing method as described previously (29). A target site was selected on the *sisold* consisting of a 5'-CCN-3' type I-A protospacer neighboring motif and a 40 nt downstream DNA sequence (protospacer). Two complementary DNA oligonucleotides were then designed based on the protospacer and synthesized. The spacer fragments were generated by annealing the corresponding complementary oligonucleotides and inserted into the BspQI site of pGE, producing plasmids carrying the artificial mini-CRISPR arrays. The donor DNA fragment was generated by splicing and overlapping extension (SOE)-PCR with *ApexHF* HS DNA Polymerase FS (Accurate Biotechnology, Hunan, China). The Donor

DNA fragments were ligated to the XhoI and SphI cleavage sites of pGE by the TEDA method(30) generating the editing plasmid.

SisOLD and its mutants were overexpressed in *Sa. islandicus* using the pSeSD vector (31,32) and in *E. coli* using the pET22b vector. PCR was used to amplify the target fragment and overlapping extension PCR was used to obtain the site-specific mutants. The *sisOLD* knockdown vector was constructed by using tandem repeats having multiple spacers. The spacer sites were chosen to contain 40 bp (TAGATTAGTTTTTCCATATCCGTTATAGCCAACGACTACG) immediately after the antisense strand GAAAG (32) and the multiple spacers were separated by the repeat sequences. The knockdown plasmid was transferred into *in situ* gene tagging of *sisold* strain for the detection of SisOLD levels with anti-Flag antibody.

Bright-field microscopy

For bright-field microscopy analysis, 5 μl of cell suspension at the indicated time points were examined under a NIKON TI-E inverted fluorescence microscope (Nikon, Japan) in Differential interference contrast (DIC) mode.

Flow cytometry analysis

The cell cycle of synchronized cells of E233S carrying pSeSD and the SisOLD overexpression plasmid was analyzed by flow cytometry using an ImageStreamX MarkII quantitative imaging analysis flow cytometer (Merk Millipore, Germany). Briefly, cells were fixed with ethanol at a final concentration of 70% for at least 12 h at each corresponding time point and stained using propidium iodide (PI) at a final concentration of 50 μg/ml. The data were collected for at least 20,000 cells per sample and analyzed using IDEAS data analysis software.

Cell cycle synchronization

In situ gene tagging of *sisOLD* strains were synchronized as previously described (27,33). Briefly, cells were first grown aerobically at 75℃ with shaking (145 rpm) in

30 ml of STVU medium. When the OD_{600} reached 0.6-0.8, the cells were transferred into 100 ml STVU medium with an initial estimated OD_{600} of 0.05 and cultivated as above. When the OD_{600} reached 0.15-0.2, acetic acid was added at a final concentration of 6 mM and the cells were blocked at G2 phase of the cell cycle after 6 h treatment. Then, the cells were collected by centrifugation at 3000 g for 10 min at room temperature to remove the acetic acid and washed twice with 0.7% (w/v) sucrose. Finally, the cells were resuspended into 100 ml of pre-warmed STVU medium and cultivated as above for subsequent analysis. For the synchronization of cells carrying plasmid for SisOLD and mutant overexpression, the ATV medium was used to induce protein expression after removal of acetic acid. The cell cycle was analyzed using flow cytometry.

Protein expression and purification

Recombinant SisOLD and mutants with C-terminal His-tag were expressed using *Escherichia coli* BL21 (DE3)-RIL cells. Protein expression was induced during logarithmic growth (OD_{600}=0.4~0.8) by the addition of 0.5 mM isopropyl-thiogalactopyranoside (IPTG) followed by an overnight cultivation at 16°C. Similarly, proteins were purified from *Sa. islandicus* using SisOLD and its mutant overexpression strains. When the overexpression strains were grown in MTV medium to OD_{600}=0.2, the expression was induced by adding arabinose and the cultivation continued for 24h. Cells were collected by centrifugation and the cell pellet was resuspended in buffer A (50 mM Tris-HCl pH 8.0, 300 mM NaCl, 5% Glycerol). Cells were lysed by sonication and the cell extract was clarified by centrifugation at 13 000 × g for 20 min at 4°C. The supernatant was incubated at 70°C for 20 min (for expression in *E. coli* only), centrifuged at 12, 000 g for 20 min again, and then filtered through a membrane filter (0.45 μm). The samples were loaded on to a Ni-NTA agarose column (Invitrogen) pre-equilibrated with buffer A and eluted with a linear imidazole (40–300 mM imidazole) gradient in buffer A. Fractions were pooled and concentrated to 1 ml and purified further by size exclusion chromatography (SEC) using a Superdex 200 column using

the buffer A (50 mM Tris-HCl pH 8.0, 300 mM NaCl, 5% Glycerol). Finally, the samples were dialyzed in a storage buffer containing 50 mM Tris–HCl pH 7.4, 100 mM NaCl, 1mM DTT, 0.1 mM EDTA and 50% glycerol. Protein concentrations were determined using the Bradford protein assay kit (Beyotime) and the purity was analyzed by 15% SDS-PAGE stained with Coomassie blue.

Western blotting

The expression levels of SisOLD and cell division proteins in the synchronized cells were analyzed by Western blotting. Around 2×10^8 cells were collected at the indicated time points for each sample and subjected to SDS-PAGE analysis in a 15% gel. The separrated proteins were then transferred onto a PVDF membrane. The specific bands were detected by chemoluminescence using Sparkjade ECL super Western blotting detection reagents (Shandong Sparkjade Biotechnology Co., Ltd.) according to the manufacturer's instructions. The primary antibodies against ESCRT-III, ESCRT-III-1, and TBP were produced in rabbit (HuaAn Biotechnology Co., Hangzhou, Zhejiang, China)(22,33), and the primary antibody against Flag tag and His tag were purchased from TransGen Biotech company (Beijing, China). The goat anti-rabbit antibodies (KermeyBiotech,Zhengzhou,China) coupled with peroxidase were used as secondary antibodies.

Electrophoretic mobility shift assay (EMSA)

The 100 nt FAM-labelled SisOLD promoter sequence (Supplementary Table S2) were used as the substrates to determine the binding capacity of aCcr1. The binding assay was performed in a 20 μL reaction mixture containing 10 nM dsDNA, 50 mM Tris-HCl, pH 7.4, 5 mM $MgCl_2$,20 mM NaCl, 50 μg/mL BSA, 1 mM DTT, 5% glycerol, and different concentrations of purified proteins. The reaction mixture was incubated at 37 °C for 30 min before loaded onto a 12% native polyacrylamide gel. After running in 0.5×TBE, the gel was visualized using an Amersham ImageQuant 800 biomolecular imager (Cytiva).

DNA cleavage assays

Supercoiled or linearized pUC19 plasmid (300 ng)was with 2 μM protein in a final volume of 20 μl in a DNA cleavage buffer (20 mM Tris-HCl pH 7.0, 50 mM KCl, 0.1 mg/ml BSA, and 10 mM divalent metal chloride salt).Reactions were carried out at 70℃ for 30 min and then the samples were quenched with 5 μl of 0.5 M EDTA, pH8.0. Samples were analyzed via native agarose electrophoresis. The signal of the initial DNA substrate (linearized or supercoiled plasmid) was measured and quantified using the ImageJ software. The dire-directed nuclease and ATPase mutants were assayed under optimal divalent metal conditions of 10 mM $MgCl_2$ and 1 mM $CaCl_2$. The cleavage efficiency was quantified by comparing the band intensity in each lane and calculating the percentage of DNA digested relative to the control.

ATPase assays

The ATPase activity was examined using a colorimetric malachite green assay that monitored the amount of free phosphate released over time (34). The reactions in a mixture containing 0.2 μM SisOLD in 25 mM Tris-HCl pH 7.4, 100 mM NaCl, 5 mM $MgCl_2$, and 1 mM ATP in a total volume of 50 μl were carried out for at least 5 min at indicated temperatures (30, 40，50，60，70，80, or 90℃). The reaction mixture was then placed on ice and quenched with 100 μl of malachite green color reagent (14 mM ammonium molybdate, 1.3 M HCl, 0.1% (v/v) Triton X-100, and 1.5 mM malachite green) and 50 μl of 21 % (w/v) citric acid. The green compound formed by malachite green, molybdate, and free phosphate was detected by absorbance at 650 nm using spectrophotometer. A sodium phosphate standard curve was used to estimate the amount of phosphate released during ATP hydrolysis. It should be noted that above 70℃, ATP is partially hydrolyzed by heat, so the amount hydrolyzed by heat were excluded from the calculation of ATP hydrolysis activity at 70, 80, and 90℃.

Plaque assays

For the phage infection assay of *E. coli*, *sisold* sequence or *sisold* with *sire_0087* were cloned into the pET22b generating a vector for the expression of recombinant SisOLD. The plasmid was transformed into *E. coli* MG1655. A colony was picked up from the plate and grown in LB broth containing ampicillin (100 mg/ml) at 37 °C to an OD_{600} of 0.4. Protein expression was induced by the addition of 0.2 mM IPTG. After 1 hour of growth, 500 µl of bacterial culture was mixed with 10 ml of 0.5% LB top layer agar and the whole sample was poured onto an LB plate containing ampicillin (100 mg/ml) and IPTG (0.1 mM). Plates were spotted with 3 µl of six 10-fold dilutions of phage T1-T7 of 10^0-10^{-5} diluted in LB liquid medium. The plates were incubated overnight at 37°C and then imaged. The infection assay of *Sa. islandicus* REY15A was according to previous report (35).

Phylogenetic analysis

The phylogenetic analyses were similar to those previously described (27). In short, a dataset of OLD family proteins from bacteria and archaea were collected by PSI-BLAST (2 iterations against the RefSeq database at NCBI; E =1e-05)(36). The collected sequences were then clustered using MMseq2 to 90% identity over 80% of the protein length. Sequences were aligned using MAFFT v7 (37) and the resultant alignment trimmed using Trimal (38), with the gap threshold of 0.2. Maximum likelihood phylogenetic analysis was performed using IQ-Tree (39), with the best selected amino acid substitution model being LG + I + G4. The branch support was assessed using SH-aLRT (40).

Chromatin fractionation

Chromatin fractionation analyses were similar to those previously described (41). In brief, the cells were harvested from the cultures at OD_{600} = 0.4 for exponential samples and OD_{600} = 1.0 for stationary samples. The cells were resuspended in 100 µl/1 OD_{600} unit/ml of chromatin extraction buffer (25 mM HEPES, 15 mM $MgCl_2$, 100 mM NaCl, 400 mM sorbitol, 0.5% Triton X-100, pH 7.5) and incubated on ice for 10 minutes. The

extracts were centrifuged for 20 minutes at 14,000 *g*, 4 ℃. The soluble fraction was transferred to a new tube and the pelleted chromatin fraction was resuspended in a volume of chromatin extraction buffer equivalent to the soluble fraction. The chromatin fraction was then sonicated three times for 30 s each.

Immunoprecipitation and mass spectrometry

1L of *Sa. islandicus* culture (SisOLD *in situ* Flag-tagged strain) in logarithmic growth phase (OD_{600}=0.3~0.6) was collected. The cells were suspended in 1 mL of lysis buffer (50 mTris-HCl, pH6.8, 150 mM NaCl, 0.1 mM DTT, 10%, w/v, glycerol, 0.5%) containing protease inhibitor PMSF (Sigma-Aldrich). The cells were broken by ultrasonication. The sample was centrifugated at 20,000×*g* at 4°C for 30 min and the supernatant was collected and used as the crude extract (input). Then RNase A was added into 500 μL of crude cell extract. The sample incubated on ice for 30 min to remove RNA. Next 50 μL anti-FLAG® M2 magnetic beads (Sigma-Aldrich) were added to the sample and the tube was incubated at 4°C with shaking for 1 hr. The beads were collected by using the magnetic rack and the supernatant (FT, flow through) was discarded. The magnetic beads were washed 5 times with lysis buffer. Finally, the proteins were eluted with 100 μl of 0.1 M glycine HCl, pH 3.0. The eluate was added into 10 μl Tris (1M), pH 8.0 to protect the eluted proteins from prolonged periods of time in the pH 3.0 solution. For The eluate sample was added into 20 μL of 5× loading buffer (100 mM Tris-HC1, pH 6.8, 200 mM β-mercaptoethanol, 4% SDS, 0.2% bromophenol blue, 20% glycerol). After boiled for 10 min, the tube was centrifugated and the supernatant was subjected for SDS-PAGE. The bands were sliced and subjected for LC-MS analysis at Beijing Protein Innovation Co., Ltd. The identified proteins are listed in Supplementary Table S3.

RESULTS

Phylogenetic diversity of OLD family proteins

All currently functionally characterized OLD family enzymes, assigned to four classes, are encoded by bacteria or bacterial viruses and are implicated in antiviral defense (1). To assess the diversity and taxonomic spread of this protein family, we assembled a dataset of OLD family proteins from bacteria and archaea and performed maximum likelihood phylogenetic analysis. Notably, not all four classes of characterized OLD family proteins were monophyletic. In particular, Class 2 enzymes were nested within the diversity of Class 1 proteins, whereas Class 4 proteins in which the ATPase and nuclease domains are split, were nested within Class 3, as a sister group to subgroup 3b. These observations are consistent with the notion that new defense systems evolve through shuffling of different modules through recombination (42). Whereas Classes 1 and 2 were distributed in both prokaryotic domains, Classes 3 and 4 were restricted to bacteria. Notably, phylogenetic analysis uncovered at least 11 well-supported, previously uncharacterized clades (U1-U11) of OLD family proteins (Fig. 1A). Two of these clades (U1 and U2) included both bacterial and archaeal representatives, five clades (U5, U6, U7, U9 and U10) were dominated by diverse bacterial sequences and four clades (U3, U4, U8 and U11) had nearly exclusively archaeal membership. Mixed phyletic patterns (e.g., mixed bacterial and archaeal membership) observed in some of the clades are consistent with the horizontal spread characteristic of defense systems (43). By contrast, clades U8 and U11 were homogeneous in their taxonomic representation, restricted to hyperhalophilic (order Halobacteriales) and thermoacidophilic (order Sulfolobales) archaea, respectively. Notably, the phylogenetic relationship between the OLD family sequences in U11 fully recapitulated the species tree of Sulfolobales (Fig. 1B) (44), suggesting conservation and vertical inheritance of the corresponding genes in this archaeal order, without obvious signs of horizontal gene transfer. Intrigued by such atypical conservation of the potential OLD family defense genes in Sulfolobales, we set out to characterize them functionally.

Sulfolobales OLD proteins have expected domain organization and are catalytically active

Analysis of a representative structural model of the Sulfolobales OLD proteins revealed a domain organization typical of this protein family, with the N-terminal ABC family ATPase and the C-terminal TOPRIM nuclease domains. Akin to most other OLD family ATPases, with a notable exception of Class 1 enzymes, Sulfolobales OLD proteins have an α-helical insertion within the TOPRIM domain (Figure 2A and 2B). Multiple sequence alignment of the Sulfolobales OLD homologs has shown that all active site residues in both ATPase and nuclease domains are conserved (Fig. S1), suggesting that the protein is enzymatically active.

To test the *in vitro* activities of Sulfolobales OLD experimentally, we focused on an OLD protein SiRe_0086 encoded by *Sa. islandicus* REY15A (SisOLD), a thermoacidophilic archaeon growing optimally at 76-80°C and pH of 2-3. The SisOLD protein was expressed and purified from *Sa. islandicus* cells (Figure 2C). Notably, whereas OLD family ATPases typically form dimers, in the gel filtration chromatography analysis, SisOLD eluted at a peak of 15.1 ml (Figure S2A), corresponding to a monomeric form (55 kDa).

Nuclease activity. The TOPRIM domain nucleases usually require divalent metal ions for catalysis (45). Thus, we examined the nuclease activity using supercoiled and linearized forms of plasmid pUC19 as the substrates in a buffer containing different divalent metal ions (Figure 2D). In the presence of 10 mM Mn^{2+} and Co^{2+}, SisOLD exhibited strong nickase activity, cleaving nearly 100% of the substrate within 20 min (Figure 2D). In the presence Mg^{2+}, ~70% of the supercoiled pUC19 plasmid substrate was nicked within 20 min. By contrast, very week activity was detected in the presence of Ni^{2+} and no activity was observed with Ca^{2+} and Zn^{2+} as the cofactor (Figure 2D). These data indicate that divalent cations are required for SisOLD activity. Notably, Ca^{2+} alone does not promote nuclease activity on supercoiled DNA substrates; however, with

a combination of Ca^{2+} and Mg^{2+}, the activity of SisOLD was higher than with either of these ions alone (Figure S2B). The enzyme showed the strongest nuclease activity in the presence of 10 mM Mg^{2+} and 1 mM Ca^{2+}. Therefore, this combination of divalent cations was used in the subsequent experiments.

SisOLD showed strong nickase activity at broad range of temperatures (between 40°C and 70°C; Figure S2C) and pH (pH 5-10, optimum at pH 6-8; Figure S2D). Notably, neither ATP nor its derivatives (ADP, dATP, and AMP) had a measurable effect on the nuclease activity of SisOLD when added to the reaction mixtures (Figure S2E). However, the nuclease activity of SisOLD was inhibited by high salt concentrations (Figure S2F).

Our results indicate that SisOLD has similar enzymatic properties as the reported Class 2 OLD family proteins. Based on the previous reports on the mutagenesis of a Class 2 OLD family nuclease (4) and our structural modelling, we hypothesized that SisOLD also uses a two-metal ion catalytic mechanism and predicted that E338, L391, D393, and E341, E409, and E411 are responsible for the binding of metal ions A and B (Figure 3A), respectively. To test this hypothesis, we constructed three mutants, 3A (E338A/L391A/D393A), 3B (E341A/E409A/E411A), 2A2B (L391A/D393A/E409A/E411A), and purified the corresponding proteins (Figure S3A). The three mutants completely lost the nuclease activity on pUC19 plasmid (Figure 3B), suggesting that both metal binding sites are essential for the nuclease activity.

ATPase activity. Although all OLD family proteins have a typical ATPase domain, not all OLD proteins have ATPase activity (e.g., GajA) (15). To determine whether SisOLD is capable of hydrolyzing ATP, we expressed and purified SisOLD from *Sa. islandicus* and examined the ATPase activity of the SisOLD *in vitro*. As shown in Figures S3C and 3D, SisOLD has ATPase activity with an optimal activity at 70-80°C. We next assessed the role of nine conserved amino acid residues located in the functionally important regions of the SisOLD ATPase domain, including the P-loop, Q-loop, D-loop, and H-

loop (Figure 3C and S1). The proteins in which the conserved residues were individually mutated to alanine were expressed, purified (Figure S3B), and their ability to hydrolyze ATP examined (Figure S3B, Figure 3D). The T37A, H280A, and S281A mutants almost completely lost the ATPase activity (Figure 3D), with T37A being the least active. However, mutations to alanine in the other six mutants (K36A, F156A, D157A, Q158A, P248A and E249A) had little effect on the ATPase activity. Collectively, these results indicate that SisOLD is a functional representative of the OLD family endowed with both nuclease and ATPase activities. Thus, we denote the clade U11 conserved across Sulfolobales (Fig. 1) as class 5.

Sulfolobales OLD family proteins are not involved in antivirus defense

Bacterial class 2-4 OLD enzymes are encoded within conserved genomic loci including other components of the corresponding defense systems. Genomic neighborhood analysis of the Sulfolobales *OLD* genes has shown that they form a conserved potential operon with a gene encoding a predicted membrane protein of unknown function (*sire_0087* in *Sa. islandicus*; Figure S4), further distinguishing the representatives of the class 5 OLD enzymes from the four previously defined OLD classes (2,15,46-48). To study whether *Sulfolobales* OLD-family proteins are implicated in anti-virus defense, we overexpressed SisOLD alone or in combination with the putative accompanying membrane protein SiRe_0087 in *Sa. islandicus* E233S and challenged the recombinant cells with Sulfolobus tenchongensis spindle shaped virus 2 (STSV2) and Sulfolobus monocaudavirus 1 (SMV1) using a spot assay. Neither of the SisOLD overexpression strains showed detectable antiviral ability. On the contrary, the strain overexpressing SisOLD alone or in combination with the membrane protein SiRe_0087 were more sensitive to STSV2 infection than the control strain (Figure S5A). Similarly, overexpression of SisOLD alone or together with SiRe_0087 in *Escherichia coli* MG1655 did not provide detectable protection against bacteriophages T1, T2, T3, T4, T5, and T7 under the assay conditions tested (Figure S5B). These results suggest that SisOLD does not function in antiviral defense but may have other functions.

Cell cycle-dependent expression of SisOLD is essential for cell viability

We have previously observed that overexpression of aCcr1, a transcription factor that regulates the cell cycle progression in *Sa. islandicus* REY15A by suppressing the expression of a gene encoding a key cytokinesis protein CdvA, resulted in 4-fold transcriptional repression of *sisOLD* (27). Analysis of the promoter region of *sisOLD* revealed the presence of the aCcr1 recognition sequence (27). Electrophoretic mobility shift assays showed that purified aCcr1 binds to the oligonucleotides encompassing the promoter region of *sisOLD* (P_{sisold}; Figure S6), confirming that aCcr1 regulates the transcriptional expression of SisOLD.

To analyze whether SisOLD exhibits cell cycle-dependent expression at the protein level, we constructed *Sa. islandicus* REY15A strains in which the SisOLD is expressed *in situ* with a Flag-tag at the C-terminus (Figure S7A). We verified that the growth and cell morphology of the *in situ* Flag-tagged SisOLD strain are not different compared to those of the wild type (Figure S7B and S7C). Then, the cell cycle of the *in situ* Flag-tagged strain was synchronized with 6 mM acetic acid (Figure 4A), and the expression levels of SisOLD at different time points were examined by Western blotting with anti-Flag antibody. As shown in Figure 4B, SisOLD exhibited a cell cycle-dependent expression pattern, with the protein levels being the highest during the G1-S cell cycle phases (i.e., 3-6 h following the removal of acetic acid; Figure 4B). Notably, during the logarithmic growth phase, the amount of SisOLD in the cells was about five times higher than during the stationary phase (Figure 4C).

To assess the importance of SisOLD for the cell, we attempted to knock out *sisOLD* using the endogenous CRISPR-based genome editing method in *Sa. islandicus* REY15A (29). However, all attempts (at least five times) failed to yield a viable knockout clone, implying that *sisOLD* is an essential gene. The essentiality of SisOLD contrasts the dispensability of defense systems, including those that have OLD family components in bacteria, and suggests that SisOLD plays an important role for the

survival of the cell even in the absence of virus infection. Notably, unlike *sisOLD*, the gene (*sire_0087*) which forms a putative operon with *sisOLD* (Figure S4) and encodes a hypothetical membrane protein could be knocked out, and the knockout strains exhibited growth and morphology phenotypes similar to those of the wild type (Figures S8A, S8C, and S8D). However, our attempts to knock out the whole operon was unsuccessful, further suggesting that the role of SisOLD is different from bacterial OLD proteins.

To further assess the importance of SisOLD for the cell, we successfully constructed a *sisOLD* knockdown strain using the endogenous CRISPR-Cas based method (49,50). As shown in Figures S9A and S9B, the knockdown strain with four spacers targeting *sisOLD* had reduced protein level (around 50%) and exhibited apparent growth retardation. Microscopy analysis revealed that the SisOLD knockdown strain generated more (5.6%, n=504) large cells (approximately 2 μm in diameter) when compared to the control strain (0.55%, n=720) (Figure S9C). Flow cytometry profiles showed a subtle decrease in the fraction of cells containing a single chromosome copy (1C) and increase in the population of cells with two chromosome copies (2C) in SisOLD knockdown strains (Figure S9D). These results further emphasize the important role of SisOLD in *Sa. islandicus*.

The ATPase activity of SisOLD is vital for the cell cycle progression

Overexpression of SisOLD resulted in dramatic growth retardation (Figure 5A), which was associated with a considerable increase in cell size, most noticeably after 24 hours post-induction (average diameter of 4.54 μm; n=100) compared to the control cells (~1.2 μm), with 95% of the cells exhibiting 50-fold increase in volume (Figure 5B and 5C). Additionally, flow cytometry analysis showed an increase in the number of genome equivalents within the population of large cells (Figure 5D). All these phenotypes imply that SisOLD is involved in cell cycle progression. Meanwhile, overexpression of SiRe_0087 had no effect on the growth and cell morphology (Figure

S8B-D). Co-expression of SisOLD and SiRe_0087 yielded phenotypes generally similar to expression of SisOLD alone (Figure S8B-D). These results suggest that although *sire_0087* and *sisold* are putatively located in the same operon, their functions may not be directly linked or correlated. To analyze whether the cell cycle-related function of SisOLD is conserved in other members of the order Sulfolobales, we overexpressed a SisOLD ortholog from *S. acidocaldarius* DSM639 (SacOLD) in *S. islandicus* E233S. SacOLD overexpression also resulted in growth retardation, larger cell size, and increased cellular DNA content (Figure S10A-C), suggesting that the cell cycle-related function of SisOLD is conserved in Sulfolobales, consistent with the conservation of gene neighborhood of *sisOLD* in other members of the order (Figures 1B and S4).

In order to explore whether the enzymatic activities of SisOLD are important for the observed effects, we constructed strains overexpressing each of the site-directed ATPase domain mutants tested in *Sa. islandicus*. Overall, the effects of different mutants on the culture growth rates and cell morphology were consistent with the *in vitro* ATPase activity results. In particular, the strains expressing the ATPase mutants that had the strongest impacts on the ATP hydrolysis *in vitro* approached the phenotypes of control cells containing the empty vector, whereas mutants in which the ATPase activity was only mildly affected, resembled the strain overexpressing the wild type SisOLD and displayed growth retardation and increase in cell size. SisOLD(T37A) almost completely lost the ATPase activity, majority of the cells were of normal size, and their growth rate was close to that of the strain carrying the empty vector pSeSD (Figure 6A). The Sis/pSeSD-SisOLD(H280A) and Sis/pSeSD-SisOLD(S281A) also had improved growth rate compared to the cells overexpressing the wild type SisOLD (Figure 6A). Notably, however, Sis/pSeSD-SisOLD(S281A) cells were enlarged and showed irregular morphologies, such as peanut-shaped and dumbbell-like (Figure 6E). The abnormal cell morphologies are reminiscent of those reported for the strain Sis/pSeSD-SisVps4(T148A) overexpressing the dominant negative ATP hydrolysis

mutant Vps4(T148A) in which the cell division is severely inhibited (51). Given that none of the single mutants recovered the phenotype of control cells, we constructed an overexpression strain Sis/pSeSD-SisOLD(T37A/H280/S281A) combining mutations in three conserved positions important for ATP hydrolysis. The triple mutant lost the ATPase activity *in vitro* (Figure 3D) and, consistently, overexpression of this mutant *in vivo* yielded cells with morphology identical to that of the control cells (Figure 6B and 6E).

Notably, *in vitro* experiments showed that the ATPase deficient mutant T37A/H280/S281A lost the nuclease activity and the same result was obtained when the ATPase domain was deleted (Figure S3E), suggesting that active ATPase domain is indispensable for SisOLD to function as a nuclease. Unexpectedly, *Sa. islandicus* strains carrying plasmids overexpressing any of the nuclease active site mutants, which abrogate the nuclease activity *in vitro*, showed the same phenotypes as those observed in the strain overexpressing the wild-type SisOLD (Figure 6C and 6D). These results indicate that the ATPase activity but not the nuclease activity of SisOLD is essential for the normal cell cycle progression.

Overexpression of SisOLD blocks cytokinesis

Next, we synchronized the SisOLD and SisOLD-T37A/H280A/S281A overexpression strains to G2 phase, with cells harboring the empty vector pSeSD used as a control (Figure 7). To ensure sufficient protein concentration, arabinose was added to induce protein expression two hours before acetic acid removal. The control cells started to divide ~4 h following the release of the cell cycle arrest. Profiles similar to those of the control cells were obtained for the strain overexpressing the inactive SisOLD ATPase mutant SisOLD-T37A/H280A/S281A (Figure 7B). By contrast, the division of the wild type SisOLD overexpression strain was blocked. Notably, although cell cycle could not progress into the cell division phase, genome replication continued in the cells

expressing the wild type SisOLD leading to accumulation of intracellular DNA, suggesting that the cell cycle was blocked in the S phase.

SisOLD may be involved in chromatin remodeling activities in G1-S phase

To gain further insights into how SisOLD functions, we determined the intracellular localization of SisOLD by chromatin fractionation. As shown in Figure 8B, a fraction of SisOLD was associated with the chromatin in the logarithmic growth phase, whereas almost all of the protein was located in the cytoplasm during the stationary phase (Figure 8A). To assess whether SisOLD is involved in chromatin remodeling, we performed pulldown assay using genome coded Flag-tagged SisOLD as a bait, followed by identification of the purified proteins by mass spectrometry. Interestingly, multiple chromatin-associated proteins co-purified with SisOLD, with Cren7 and histone deacetylase superfamily protein (SiRe_1988) being the most abundant (Figures 8B and 8C, Supplementary Table S3). Notably, both SisOLD and Cren7 are among the essential genes co-regulated by aCcr1 (27). Given that SisOLD has active ATPase and nuclease domains, we hypothesize that it plays a role in chromatin relaxation and/or chromosome remodeling in cooperation with chromatin proteins, such as Cren7, during the S phase, facilitating replication and subsequent chromosome segregation.

DISCUSSION

Here, we characterized a representative of a new class of OLD family proteins, class 5, and the first OLD family protein from archaea. Contrary to our initial expectation, SisOLD does not appear to participate in the anti-virus defense but is rather involved in the cell cycle progression. The protein level keeps constantly high during the progression of the cell cycle from the M phase through G1 into the DNA synthesis (S) phase, but is depleted during the post-replicative G2 phase (Figure 4B). Importantly, SisOLD is enriched in the chromatin fraction in vigorously growing cells and immunoprecipitation showed that SisOLD is associated with the chromatin protein

Cren7 and a histone deacetylase homolog. These observations suggest that SisOLD probably functions during the chromosome replication. We showed that *SisOLD* gene is essential for the cell viability. In contrast, genes coding for the OLD proteins in bacteria and viruses tend to be located in defense islands (2) and are non-essential for the normal cell growth or viability.

Although SisOLD is indispensable for cell survival, the relative mildness of the phenotype of the knockdown strain may be due to the fact that cells with 50% of SisOLD level are still able to complete the cell cycle progression. However, the phenotype of the SisOLD overexpression strain strongly supports the hypothesis that this archaeal OLD protein is involved in the progression of the cell cycle. We hypothesize that during the normal cell cycle progression, SisOLD levels need to be reduced during G2 phase prior to cell division (Figure 4B), when chromosomes need to be condensed in preparation for segregation. Following the cell division, SisOLD expression is elevated and its ATP-dependent nickase activity promotes the relaxation of the chromosomes facilitating genome replication. Unexpectedly, overexpression of the nuclease deficient mutant displayed phenotype akin to the wild type. This may be due to the presence of chromosome-coded SisOLD which is sufficient for nicking the chromosome. The overexpression of SisOLD prevents chromosomal condensation and subsequent cytokinesis. Notably, however, this does not prevent the subsequent round of genome replication, further suggesting that genome replication and cytokinesis are not strictly coupled in *Sa. islandicus*, consistent with previous results (51). This could explain the emergence of large cells with multiple copies of the genome. Thus, the cells appear to be blocked in the S phase. This result is consistent with the more efficient proliferation of the STSV2 virus in the SisOLD overexpression strain. Indeed, similar to some other viruses, STSV2 is known to block the cell cycle progression in the S phase which provides the virus with the access to the host's replication machinery (35,52-54).

Structural and biochemical studies have greatly increased our understanding on the anti-

phage functions of the OLD family proteins in bacteria in recent years. In the Gabija antiviral system, a representative of the Class 2 OLD family, GajA has likely lost its ATP hydrolysis activity during evolution but retained its nucleotide-binding capacity (15). The ATPase domain may have evolved into a regulatory domain stimulating the nuclease activity in response to viral invasion (12,15). The Class 2 OLD proteins BpOLD and XccOLD, encoded by *Burkholderia pseudomallei* and *Xanthamonas campestris pv. Campestris*, respectively, catalyze the nicking and cleavage of DNA substrates in a divalent metal-dependent manner *in vitro*. Although the N-terminal ATPase domain of the latter OLD proteins is essential for the nuclease activities, it is thought primarily to promote oligomerization (4). Because in the cleavage reactions of full-length protein, the presence or absence of ATP had little effect on the cleavage activity (4), it has been speculated that the ATPase structural domain may have a regulatory function, controlling how and when the catalytic C-terminal region gains access to the substrate (4). Similarly, in our current study, we found that *in vitro* the presence or absence of ATP, dATP, ADP, and AMP does not affect the nuclease activity of SisOLD. However, deletion or inactivation of the ATPase domain through point mutations blocked the nuclease activity, indicating that there is a cross talk between the two domains. Furthermore, *in vivo*, the strains overexpressing the ATPase deficient mutants did not show growth inhibition, unlike the wild type, suggesting that the ATPase structural domain of SisOLD is crucial for its function *in vivo*. Interestingly, class 1 and class 2 OLD proteins usually exist in solution as dimers and tetramers (3,46), respectively. For instance, GajA and GajB can only perform anti-phage activity when they form a 4:4 complex (13,14,46,47). By contrast, SisOLD appears to exist *in vitro* as a monomer. The predicted structure of SisOLD lacks the dimerization module at the N-terminus compared to other Class 2 OLD proteins and this may be related to its monomeric state and function *in vivo*.

In eukaryotes, timely localization of nucleosomes along the genome is essential for global gene regulation. Histone modification is an important mechanism for regulating

genome accessibility (55). Chromatin remodeling is an active process involving large and complex ATP depletion complexes (56,57). Immunoprecipitation experiments showed that SisOLD are associated with histone deacetylase homolog and Cren7, Sac7d/Sso7d, SSB (single-stranded DNA binding protein), and Alba. Chromatin proteins have various post-translational modifications (acetylation, methylation, phosphorylation, etc.)(58), which affect not only the properties of the proteins themselves, but also the structure of the chromatin and gene expression. For example, many chromatin proteins of *Sa. islandicus* have been reported to be post-translationally acetylated or methylated (59,60). SisOLD could promote chromatin remodeling by either directly interacting with the DNA-associated proteins or through stimulation of proteins involved in post-translational modification.

The SisOLD expression is cyclically controlled, consistent with its role in the cell cycle. This is apparently achieved through a combination of transcriptional regulation by aCcr1 and degradation of the protein (23). It has been reported that the half-life of the *SSO2277* mRNA, a closely similar ortholog of SisOLD from *Saccharolobus solfataricus*, is only 3 min (61). Furthermore, there was a slight accumulation of SacOLD when the cells were treated with the proteasome inhibitor Bortezomib (23). These observations imply that the mRNA of SisOLD is tightly controlled at the transcriptional level and the level of SisOLD could be further regulated at the protein level by proteasome degradation. The dual regulation that SisOLD is subjected to *in vivo* emphasizes the importance of cell cycle phase-dependent functioning of this protein. Collectively, our study has revealed an unexpected novel function of an archaeal OLD family protein in cell cycle progression.

DATA AVAILABILITY

All data supporting the findings of this study are available within the article and its Supplementary Information, or from the corresponding author upon reasonable request.

ACKNOWLEDGEMENTS

We would like to thank members of the CRISPR and Archaea Biology Research Center for helpful discussions and technicians from the Core Facilities for Life and Environmental Sciences, State Key Laboratory of Microbial Technology of Shandong University for assistance.

FUNDING

This work was supported by National Natural Science Foundation of China [32393973 and 32370033 to Y.S. and Postdoctoral fellowship Program of CPSF (GZC20231471) and Postdoc Innovation Project of Shandong Province (SDCX-ZG-202400122) to Y.Y.

References

1. Dot, E.W., Thomason, L.C. and Chappie, J.S. (2023) Everything OLD is new again: How structural, functional, and bioinformatic advances have redefined a neglected nuclease family. *Mol Microbiol*, **120**, 122-140.
2. Akritidou, K. and Thurtle-Schmidt, B.H. (2023) OLD family nuclease function across diverse anti-phage defense systems. *Front Microbiol*, **14**.
3. Schiltz, C.J., Adams, M.C. and Chappie, J.S. (2020) The full-length structure of OLD defines the ATP hydrolysis properties and catalytic mechanism of Class 1 OLD family nucleases. *Nucleic Acids Res*, **48**, 2762-2776.
4. Schiltz, C.J., Lee, A., Partlow, E.A., Hosford, C.J. and Chappie, J.S. (2019) Structural characterization of Class 2 OLD family nucleases supports a two-metal catalysis mechanism for cleavage. *Nucleic Acids Res*, **47**, 9448-9463.
5. Aravind, L., Leipe, D.D. and Koonin, E.V. (1998) Toprim - a conserved catalytic domain in type IA and II topoisomerases, DnaG-type primases, OLD family nucleases and RecR proteins. *Nucleic Acids Res*, **26**, 4205-4213.
6. Lindahl, G., Sironi, G., Bialy, H. and Calendar, R. (1970) Bacteriophage Lambda - Abortive Infection of Bacteria Lysogenic for Phage-P2. *P Natl Acad Sci USA*, **66**, 587-&.
7. Doron, S., Melamed, S., Ofir, G., Leavitt, A., Lopatina, A., Keren, M., Amitai, G. and Sorek, R. (2018) Systematic discovery of antiphage defense systems in the microbial pangenome. *Science*, **359**.
8. Gao, L.Y., Altae-Tran, H., Böhning, F., Makarova, K.S., Segel, M., Schmid-Burgk, J.L., Koob, J., Wolf, Y.I., Koonin, E.V. and Zhang, F. (2020) Diverse enzymatic activities mediate antiviral immunity in prokaryotes. *Science*, **369**, 1077-+.
9. Mestre, M.R., González-Delgado, A., Gutierrez-Rus, L.I., Martínez-Abarca, F. and Toro, N. (2020) Systematic prediction of genes functionally associated with bacterial retrons and classification of the encoded tripartite systems. *Nucleic Acids Res*, **48**, 12632-12647.

10. Millman, A., Bernheim, A., Stokar-Avihail, A., Fedorenko, T., Voichek, M., Leavitt, A., Oppenheimer-Shaanan, Y. and Sorek, R. (2020) Bacterial Retrons Function In Anti-Phage Defense. *Cell*, **183**, 1551-+.
11. Rousset, F., Depardieu, F., Miele, S., Dowding, J., Laval, A.L., Lieberman, E., Garry, D., Rocha, E.P.C., Bernheim, A. and Bikard, D. (2022) Phages and their satellites encode hotspots of antiviral systems. *Cell Host Microbe*, **30**, 740-+.
12. Cheng, R., Huang, F.T., Lu, X.L., Yan, Y., Yu, B.B., Wang, X.L. and Zhu, B. (2023) Prokaryotic Gabija complex senses and executes nucleotide depletion and DNA cleavage for antiviral defense. *Cell Host Microbe*, **31**.
13. Antine, S.P., Johnson, A.G., Mooney, S.E., Leavitt, A., Mayer, M.L., Yirmiya, E., Amitai, G., Sorek, R. and Kranzusch, P.J. (2024) Structural basis of Gabija anti-phage defence and viral immune evasion. *Nature*, **625**.
14. Yang, X.Y., Shen, Z.F., Xie, J.L., Greenwald, J., Marathe, I., Lin, Q.P., Xie, W.J., Wysocki, V.H. and Fu, T.M. (2024) Molecular basis of Gabija anti-phage supramolecular assemblies. *Nat Struct Mol Biol*.
15. Cheng, R., Huang, F.T., Wu, H., Lu, X.L., Yan, Y., Yu, B.B., Wang, X.L.E. and Zhu, B. (2021) A nucleotide-sensing endonuclease from the Gabija bacterial defense system. *Nucleic Acids Res*, **49**, 5216-5229.
16. Spang, A., Caceres, E.F. and Ettema, T.J.G. (2017) MICROBIAL GENOMICS Genomic exploration of the diversity, ecology, and evolution of the archaeal domain of life. *Science*, **357**.
17. Liu, Y., Makarova, K.S., Huang, W.C., Wolf, Y.I., Nikolskaya, A.N., Zhang, X.X., Cai, M.W., Zhang, C.J., Xu, W., Luo, Z.H. *et al.* (2021) Expanded diversity of Asgard archaea and their relationships with eukaryotes. *Nature*, **593**, 553-+.
18. Imachi, H., Nobu, M.K., Nakahara, N., Morono, Y., Ogawara, M., Takaki, Y., Takano, Y., Uematsu, K., Ikuta, T., Ito, M. *et al.* (2020) Isolation of an archaeon at the prokaryote-eukaryote interface. *Nature*, **577**, 519-+.
19. Lundgren, M. and Bernander, R. (2005) Archaeal cell cycle progress. *Curr Opin Microbiol*, **8**, 662-668.
20. Lundgren, M., Malandrin, L., Eriksson, S., Huber, H. and Bernander, R. (2008) Cell cycle characteristics of

:: Unity among diversity. *J Bacteriol*, **190**, 5362-5367.

21. Lindås, A.C. and Bernander, R. (2013) The cell cycle of archaea. *Nat Rev Microbiol*, **11**, 627-638.
22. Liu, J.F., Gao, R.X., Li, C.T., Ni, J.F., Yang, Z.J., Zhang, Q., Chen, H.N. and Shen, Y.L. (2017) Functional assignment of multiple ESCRT-III homologs in cell division and budding in. *Mol Microbiol*, **105**, 540-553.
23. Risa, G.T., Hurtig, F., Bray, S., Hafner, A.E., Harker-Kirschneck, L., Faull, P., Davis, C., Papatziamou, D., Mutavchiev, D.R., Fan, C. *et al.* (2020) The proteasome controls ESCRT-III-mediated cell division in an archaeon. *Science*, **369**, 642-+.
24. Samson, R.Y., Obita, T., Freund, S.M., Williams, R.L. and Bell, S.D. (2008) A Role for the ESCRT System in Cell Division in Archaea. *Science*, **322**, 1710-1713.
25. Lindås, A.C., Karlsson, E.A., Lindgren, M.T., Ettema, T.J.G. and Bernander, R. (2008) A unique cell division machinery in the Archaea. *P Natl Acad Sci USA*, **105**, 18942-18946.
26. Li, X.Y., Lozano-Madueno, C., Martinez-Alvarez, L. and Peng, X. (2023) A clade of RHH proteins ubiquitous in Sulfolobales and their viruses regulates cell cycle progression (vol 51, pg 1724, 2023). *Nucleic Acids Res*, **51**, 4100-4100.

27. Yang, Y.F., Liu, J.F., Fu, X.F., Zhou, F., Zhang, S., Zhang, X.M., Huang, Q.H., Krupovic, M., She, Q.X., Ni, J.F. *et al.* (2023) A novel RHH family transcription factor aCcr1 and its viral homologs dictate cell cycle progression in archaea. *Nucleic Acids Res*, **51**, 1707-1723.
28. Deng, L., Zhu, H.J., Chen, Z.J., Liang, Y.X. and She, Q.X. (2009) Unmarked gene deletion and host-vector system for the hyperthermophilic crenarchaeon Sulfolobus islandicus. *Extremophiles*, **13**, 735-746.
29. Li, Y.J., Pan, S.F., Zhang, Y., Ren, M., Feng, M.X., Peng, N., Chen, L.M., Liang, Y.X. and She, Q.X. (2016) Harnessing Type I and Type III CRISPR-Cas systems for genome editing. *Nucleic Acids Res*, **44**.
30. Xia, Y.Z., Li, K., Li, J.J., Wang, T.Q., Gu, L.C. and Xun, L.Y. (2019) T5 exonuclease-dependent assembly offers a low-cost method for efficient cloning and site-directed mutagenesis. *Nucleic Acids Res*, **47**.
31. Peng, N., Deng, L., Mei, Y.X., Jiang, D.Q., Hu, Y.M., Awayez, M., Liang, Y.X. and She, Q.X. (2012) A Synthetic Arabinose-Inducible Promoter Confers High Levels of Recombinant Protein Expression in Hyperthermophilic Archaeon. *Appl Environ Microb*, **78**, 5630-5637.
32. Peng, N., Han, W.Y., Li, Y.J., Liang, Y.X. and She, Q.X. (2017) Genetic technologies for extremely thermophilic microorganisms of

, the only genetically tractable genus of crenarchaea. *Sci China Life Sci*, **60**, 370-385.
33. Liu, J.F., Cvirkaite-Krupovic, V., Commere, P.H., Yang, Y.F., Zhou, F., Forterre, P., Shen, Y.L. and Krupovic, M. (2021) Archaeal extracellular vesicles are produced in an ESCRT-dependent manner and promote gene transfer and nutrient cycling in extreme environments. *Isme J*, **15**, 2892-2905.
34. Monroe, N., Han, H., Gonciarz, M.D., Eckert, D.M., Karren, M.A., Whitby, F.G., Sundquist, W.I. and Hill, C.P. (2014) The Oligomeric State of the Active Vps4 AAA ATPase. *J Mol Biol*, **426**, 510-525.
35. Liu, J.F., Cvirkaite-Krupovic, V., Baquero, D.P., Yang, Y.F., Zhang, Q., Shen, Y.L. and Krupovic, M. (2021) Virus-induced cell gigantism and asymmetric cell division in archaea. *P Natl Acad Sci USA*, **118**.
36. Altschul, S.F., Madden, T.L., Schaffer, A.A., Zhang, J.H., Zhang, Z., Miller, W. and Lipman, D.J. (1997) Gapped BLAST and PSI-BLAST: a new generation of protein database search programs. *Nucleic Acids Res*, **25**, 3389-3402.
37. Katoh, K., Rozewicki, J. and Yamada, K.D. (2019) MAFFT online service: multiple sequence alignment, interactive sequence choice and visualization. *Brief Bioinform*, **20**, 1160-1166.
38. Capella-Gutiérrez, S., Silla-Martínez, J.M. and Gabaldón, T. (2009) trimAl: a tool for automated alignment trimming in large-scale phylogenetic analyses. *Bioinformatics*, **25**, 1972-1973.
39. Minh, B.Q., Schmidt, H.A., Chernomor, O., Schrempf, D., Woodhams, M.D., von Haeseler, A. and Lanfear, R. (2020) IQ-TREE 2: New Models and Efficient Methods for Phylogenetic Inference in the Genomic Era. *Mol Biol Evol*, **37**, 1530-1534.
40. Guindon, S., Dufayard, J.F., Lefort, V., Anisimova, M., Hordijk, W. and Gascuel, O. (2010) New Algorithms and Methods to Estimate Maximum-Likelihood Phylogenies: Assessing the Performance of PhyML 3.0. *Syst Biol*, **59**, 307-321.
41. Takemata, N., Samson, R.Y. and Bell, S.D. (2019) Physical and Functional Compartmentalization of Archaeal Chromosomes. *Cell*, **179**, 165-+.
42. Koonin, E.V., Makarova, K.S. and Wolf, Y.I. (2017) Evolutionary Genomics of Defense Systems in Archaea and Bacteria. *Annu Rev Microbiol*, **71**, 233-+.
43. Rocha, E.P.C. and Bikard, D. (2022) Microbial defenses against mobile genetic elements and viruses: Who defends whom from what? *Plos Biol*, **20**.

44. Counts, J.A., Willard, D.J. and Kelly, R.M. (2021) Life in hot acid: a genome-based reassessment of the archaeal order. *Environ Microbiol*, **23**, 3568-3584.
45. Yang, W. (2011) Nucleases: diversity of structure, function and mechanism. *Q Rev Biophys*, **44**, 1-93.
46. Huo, Y.W., Kong, L.F., Zhang, Y., Xiao, M., Du, K., Xu, S.Y.T., Yan, X.X., Ma, J. and Wei, T.T. (2024) Structural and biochemical insights into the mechanism of the Gabija bacterial immunity system. *Nat Commun*, **15**.
47. Li, J., Cheng, R., Wang, Z.M., Yuan, W.L., Xiao, J., Zhao, X.Y., Du, X.R., Xia, S.Y., Wang, L.R., Zhu, B. *et al.* (2024) Structures and activation mechanism of the Gabija anti-phage system. *Nature*.
48. Oh, H., Koo, J., An, S.Y., Hong, S.H., Suh, J.Y. and Bae, E. (2023) Structural and functional investigation of GajB protein in Gabija anti-phage defense. *Nucleic Acids Res*, **51**, 11941-11951.
49. Peng, W.F., Feng, M.X., Feng, X., Liang, Y.X. and She, Q.X. (2015) An archaeal CRISPR type III-B system exhibiting distinctive RNA targeting features and mediating dual RNA and DNA interference. *Nucleic Acids Res*, **43**, 406-417.
50. Zink, I.A., Pfeifer, K., Wimmer, E., Sleytr, U.B., Schuster, B. and Schleper, C. (2019) CRISPR-mediated gene silencing reveals involvement of the archaeal S-layer in cell division and virus infection. *Nat Commun*, **10**.
51. Liu, J.F., Lelek, M., Yang, Y.F., Salles, A., Zimmer, C., Shen, Y.L. and Krupovic, M. (2025) A relay race of ESCRT-III paralogs drives cell division in a hyperthermophilic archaeon. *Mbio*, **16**.
52. Kiro, R., Molshanski-Mor, S., Yosef, I., Milam, S.L., Erickson, H.P. and Qimron, U. (2013) Gene product 0.4 increases bacteriophage T7 competitiveness by inhibiting host cell division. *P Natl Acad Sci USA*, **110**, 19549-19554.
53. Stewart, C.R., Deery, W.J., Egan, E.S.K., Myles, B. and Petti, A.A. (2013) The product of SPO1 gene 56 inhibits host cell division during infection of
by bacteriophage SPO1. *Virology*, **447**, 249-253.
54. Fan, Y., Sanyal, S. and Bruzzone, R. (2018) Breaking Bad: How Viruses Subvert the Cell Cycle. *Front Cell Infect Mi*, **8**.
55. Bannister, A.J. and Kouzarides, T. (2011) Regulation of chromatin by histone modifications. *Cell Res*, **21**, 381-395.
56. Vignali, M., Hassan, A.H., Neely, K.E. and Workman, J.L. (2000) ATP-dependent chromatin-remodeling complexes. *Mol Cell Biol*, **20**, 1899-1910.
57. Narlikar, G.J., Sundaramoorthy, R. and Owen-Hughes, T. (2013) Mechanisms and Functions of ATP-Dependent Chromatin-Remodeling Enzymes. *Cell*, **154**, 490-503.
58. Wolffe, A.P. and Hayes, J.J. (1999) Chromatin disruption and modification. *Nucleic Acids Res*, **27**, 711-720.
59. Vorontsov, E.A., Rensen, E., Prangishvili, D., Krupovic, M. and Chamot-Rooke, J. (2016) Abundant Lysine Methylation and N-Terminal Acetylation in
Revealed by Bottom-Up and Top-Down Proteomics. *Mol Cell Proteomics*, **15**, 3388-3404.
60. Cao, J.J., Wang, T.K., Wang, Q., Zheng, X.W. and Huang, L. (2019) Functional Insights Into Protein Acetylation in the Hyperthermophilic Archaeon. *Mol Cell Proteomics*, **18**, 1572-1587.
61. Andersson, A.F., Lundgren, M., Eriksson, S., Rosenlund, M., Bernander, R. and Nilsson, P. (2006) Global analysis of mRNA stability in the archaeon. *Genome Biol*, **7**.

FIGURES LEGENDS

Figure 1. Diversity of OLD family proteins in bacteria and archaea. (**A**) Maximum likelihood phylogenetic analysis of OLD family proteins. The tree was midpoint rooted. Previously characterized groups of OLD family proteins are denoted by Classes 1 through 4, whereas the clades encompassing uncharacterized protein sequences are labeled U1-U11. (**B**) Detailed view of the U11 clade including OLD family proteins conserved in Sulfolobales. In both panels, well supported clades were collapsed to triangles, whose side lengths are proportional to the distances between closest and farthest leaf nodes. The scale bars represent the number of substitutions per site, whereas blue circles denote aLRT branch supports higher than 90.

Figure 2. SisOLD exhibits metal-dependent nuclease activity *in vitro*. (**A**) Domain architecture of SisOLD. Sis^{CTR}, the C-terminal domain of SisOLD. (**B**) Structure of SisOLD predicted by Alpha fold2. The domains are shown in different colors as in (A). (**C**) SDS-PAGE showing purified full-length SisOLD. (**D**) Metal-dependent nuclease activity of SisOLD on supercoiled pUC19. 'N', 'L', and 'S' denote the positions of 'nicked', 'linearized', and 'supercoiled' DNA, respectively.

Figure 3. SisOLD nuclease active site and ATPase key site mutants. (**A**) Metal ion binding residues in the structural domains of nucleases predicted based on protein structure and sequence. (**B**) Analysis of nickase activity of key residue combination mutants 3A, 3B, 2A2B of nuclease in vitro. 3A represents the E338A, L391A, D393A combination mutation, 3B represents the E341A, E409A, E411A combination mutation, and 2A2B represents the L391A, D393A, E409A, E411A combination mutation. 'N', 'L', and 'S' denote the positions of 'nicked', 'linearized', and 'supercoiled' DNA, respectively. (**C**) Key loops of the ATPase structural domain binding as well as the active center of hydrolysis of SisOLD based on protein structure and sequence

prediction. (**D**) Analysis of ATP hydrolytic activity of mutants of key amino acids of ATPase in vitro.

Figure 4. The cyclically expressed gene *sisold* is essential for cell viability. (**A**) Flow cytometry profiles of samples of a synchronized SisOLD in-situ-flag strain in one cell cycle. The cells were synchronized at G2 phase after treated with 6 mM acetic acid for 6 h before released by removing the acetic acid. The cultures were collected at different time points (0, 1.0, 2.0, 3.0, 4.0, 5.0, 6.0 and 7.0 h) and subjected to flow cytometry analysis. Cells started to divide at 2.0h as shown by the appearance of cells with one copy chromosome (1C) and the ratio of dividing cells reached the highest level at about 3–3.5 h. As the cell cycle proceeded, cells with two copy chromosomes (2C) became dominant at 6h. (**B**) Changes of the protein levels of SisOLD during a cell cycle detected by Western blotting using anti-Flag antibody. The known periodic expression of CdvB and CdvB1 were used as positive controls, and TBP (TATA-box binding protein) was used as a loading control. (**C**) Western blotting analysis showing the differences in the protein levels of SisOLD during the exponential (OD_{600}=0.4) and stable (OD_{600}=1.0) phases.

Figure 5. Overexpression of SisOLD leads to retarded cell growth and cell enlargement. (**A**) Growth curves of cells over-expressing the C-terminal His-tagged SisOLD. The cells were inoculated into 30 ml induction medium ATV to a final estimated OD_{600} of 0.03. The growth was monitored at OD_{600}. Each value was based on data from three independent measurements. Cells harboring the empty plasmid pSeSD were used as a control. (**B**) Bright-field microscopy (DIC) of cells over-expressing SisOLD. Cells cultured in the induction medium were taken at different time points and observed under a NIKON-E microscope. Upper, middle, and lower panels, 0, 12, and 24h. Scale bars: 2 μm. (**C**) Cell size statistics of the data in (B). Cell cultures were sampled at the indicated time points and observed under the microscope. The

diameters of ~100 cells were measured using ImageJ software for each culture repeat. (**D**) Flow cytometry analysis of the DNA content of Sis/pSeSD and Sis/pSeSD-SisOLD cells cultured in MATV medium.

Figure 6. The ATPase activity of SisOLD is vital for cell cycle progression. (**A**) Overexpression growth curve analysis of a single ATPase key amino acid mutant. (**B**) Overexpression growth curve anaysis of T37，H280 and S281 combination mutants. (**C**) Growth curves of metal ion binding site mutant overexpression strains. 3A represents the E338A，L391A，D393A combination mutation, 3B represents the E341A，E409A，E411A combination mutation, and 2A2B represents the L391A，D393A，E409A，E411A combination mutation. (**D**)indicates the cellular morphology of the overexpression strain in (C), taken from a sample induced by arabinose for 24h; Scale bars: 2 μm. (**E**) Cell morphology analysis of overexpression strains in (A) and (B). Samples were taken from arabinose induction for 24h; Scale bars: 2 μm.

Figure 7. Overexpression of SisOLD blocks the process of cell division. (**A**) A schematic showing cell synchronization and induction of SisOLD over-expression with arabinose (0.2%). The time for the acetic acid treatment and arabinose induction are indicated. E233S containing the empty plasmid (Sis/pSeSD) was used as a control. (**B**) Flow cytometry profiles of DNA content distribution of cells 0-5 hrs after acetic acid removal.

Figure 8. Subcellular localization and analysis of the cellular amount as well as associated proteins. (**A**) Cellular localization of SisOLD in the cytoplasm or chromatin of cells during the exponential phase (OD_{600}=0.4) of cell growth as well as in stationary cells (OD_{600}=1.0). T, total protein. C, Chromatin fractions. S, Soluble fractions. (**B**) SDS-PAGE and (**C**) Western blotting of immunoprecipitation of SisOLD *in-situ* Flag strains. Input represents cell lysate, FT indicates flow-through, Wash indicates washing

of magnetic beads using buffer A to remove nonspecifically bound fractions and elute indicates elution fractions of target proteins.

FIGURES

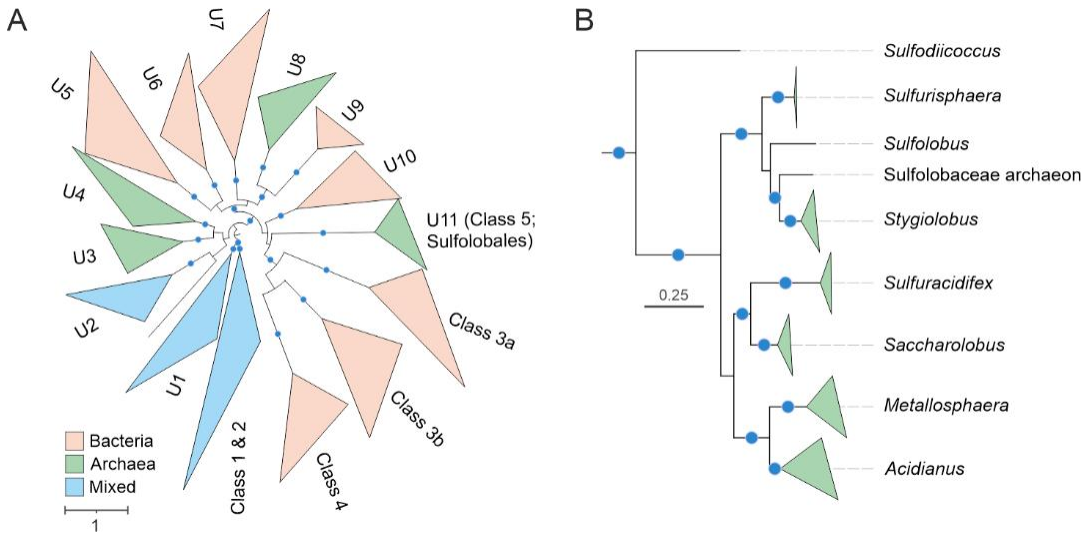

Figure 1. Diversity of OLD family proteins in bacteria and archaea. (**A**) Maximum likelihood phylogenetic analysis of OLD family proteins. The tree was midpoint rooted. Previously characterized groups of OLD family proteins are denoted by Classes 1 through 4, whereas the clades encompassing uncharacterized protein sequences are labeled U1-U11. (**B**) Detailed view of the U11 clade including OLD family proteins conserved in Sulfolobales. In both panels, well supported clades were collapsed to triangles, whose side lengths are proportional to the distances between closest and farthest leaf nodes. The scale bars represent the number of substitutions per site, whereas blue circles denote aLRT branch supports higher than 90.

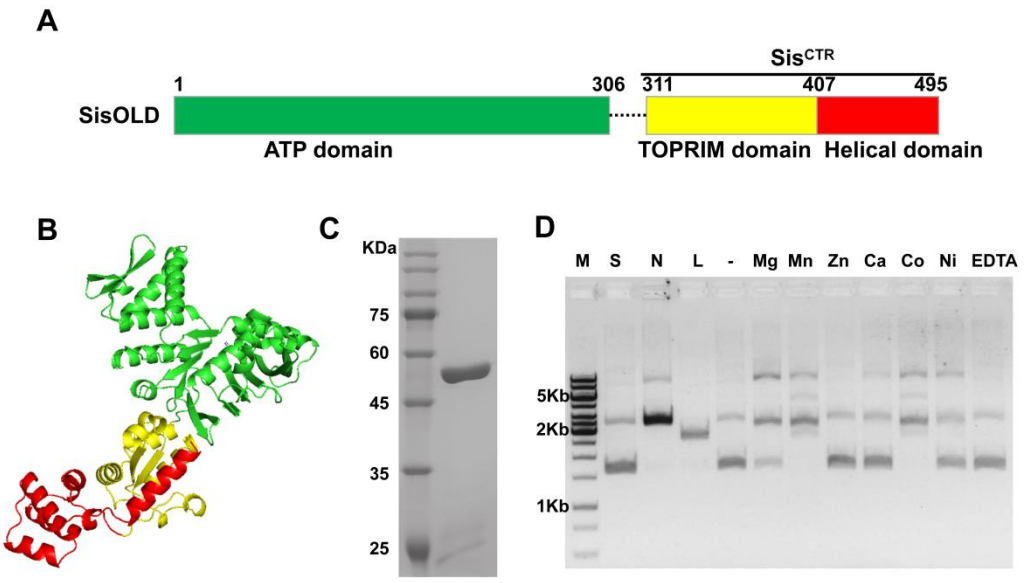

Figure 2. SisOLD exhibits metal-dependent nuclease activity *in vitro*. (**A**) Domain architecture of SisOLD. Sis^{CTR}, the C-terminal domain of SisOLD. (**B**) Structure of SisOLD predicted by Alpha fold2. The domains are shown in different colors as in (A). (**C**) SDS-PAGE showing purified full-length SisOLD. (**D**) Metal-dependent nuclease activity of SisOLD on supercoiled pUC19. 'N', 'L', and 'S' denote the positions of 'nicked', 'linearized', and 'supercoiled' DNA, respectively.

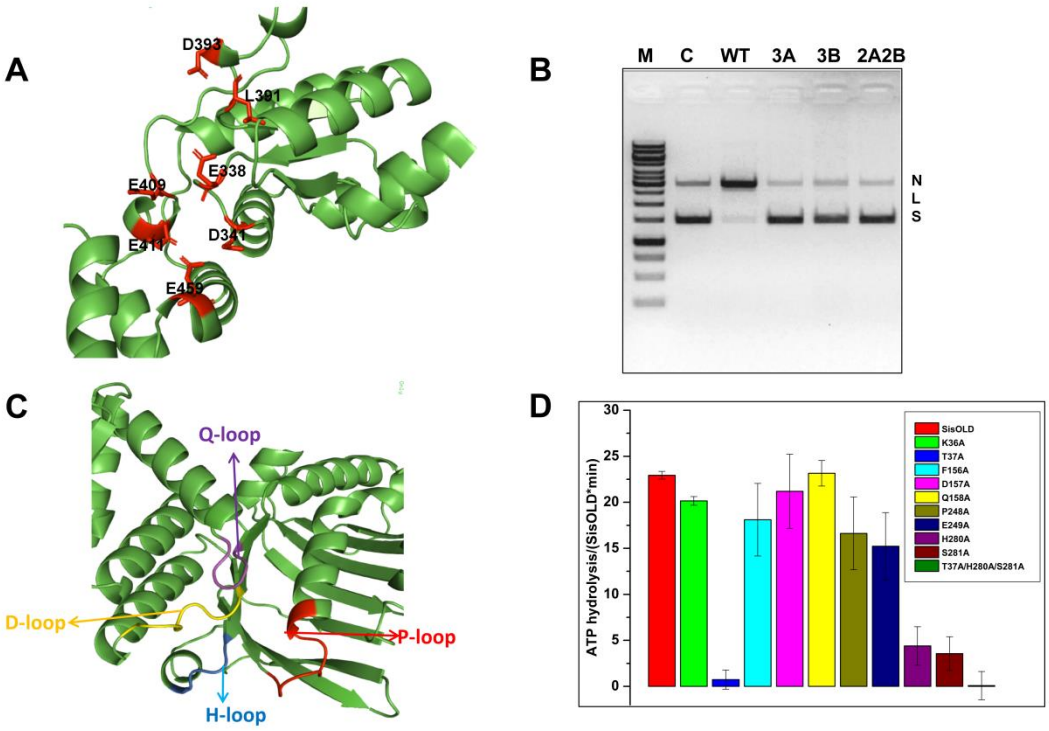

Figure 3. SisOLD nuclease active site and ATPase key site mutants. (**A**) Metal ion binding residues in the structural domains of nucleases predicted based on protein structure and sequence. (**B**) Analysis of nickase activity of key residue combination mutants 3A, 3B, 2A2B of nuclease in vitro. 3A represents the E338A, L391A, D393A combination mutation, 3B represents the E341A, E409A, E411A combination mutation, and 2A2B represents the L391A, D393A, E409A, E411A combination mutation. 'N', 'L', and 'S' denote the positions of 'nicked', 'linearized', and 'supercoiled' DNA, respectively. (**C**) Key loops of the ATPase structural domain binding as well as the active center of hydrolysis of SisOLD based on protein structure and sequence prediction. (**D**) Analysis of ATP hydrolytic activity of mutants of key amino acids of ATPase in vitro.

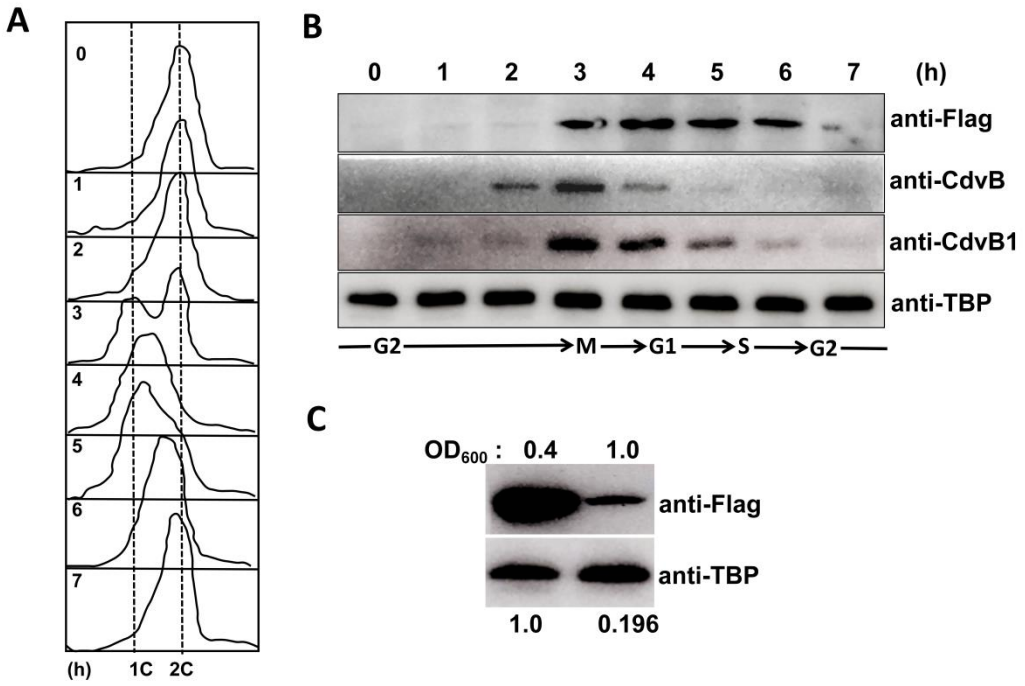

Figure 4. The cyclically expressed gene *sisold* is essential for cell viability. (**A**) Flow cytometry profiles of samples of a synchronized SisOLD in-situ-flag strain in one cell cycle. The cells were synchronized at G2 phase after treated with 6 mM acetic acid for 6 h before released by removing the acetic acid. The cultures were collected at different time points (0, 1.0, 2.0, 3.0, 4.0, 5.0, 6.0 and 7.0 h) and subjected to flow cytometry analysis. Cells started to divide at 2.0h as shown by the appearance of cells with one copy chromosome (1C) and the ratio of dividing cells reached the highest level at about 3–3.5 h. As the cell cycle proceeded, cells with two copy chromosomes (2C) became dominant at 6h. (**B**) Changes of the protein levels of SisOLD during a cell cycle detected by Western blotting using anti-Flag antibody. The known periodic expression of CdvB and CdvB1 were used as positive controls, and TBP (TATA-box binding protein) was used as a loading control. (**C**) Western blotting analysis showing the differences in the protein levels of SisOLD during the exponential (OD_{600}=0.4) and stable (OD_{600}=1.0) phases.

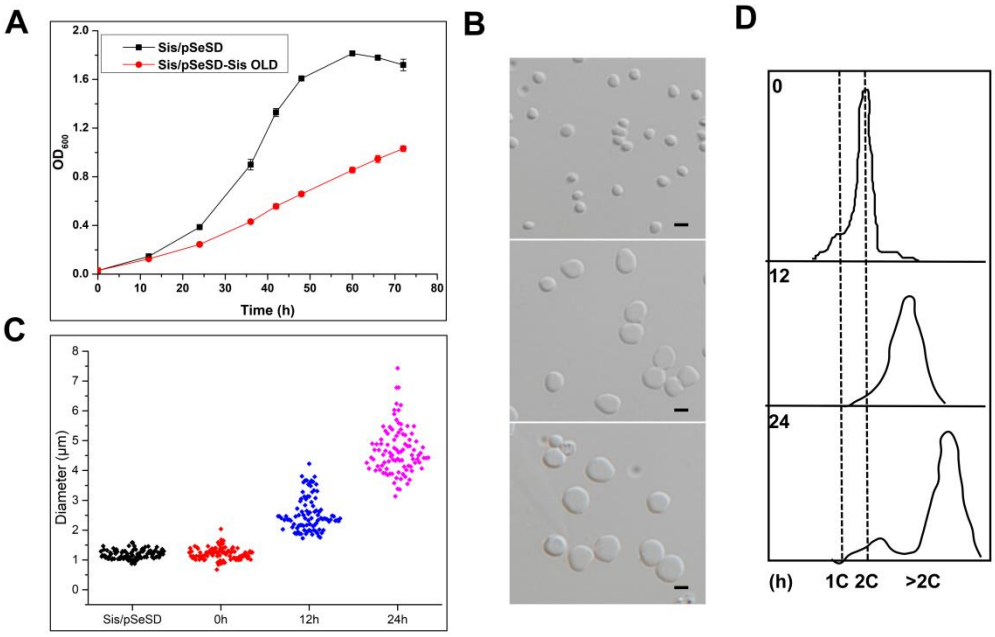

Figure 5. Overexpression of SisOLD leads to retarded cell growth and cell enlargement. (**A**) Growth curves of cells over-expressing the C-terminal His-tagged SisOLD. The cells were inoculated into 30 ml induction medium ATV to a final estimated OD_{600} of 0.03. The growth was monitored at OD_{600}. Each value was based on data from three independent measurements. Cells harboring the empty plasmid pSeSD were used as a control. (**B**) Bright-field microscopy (DIC) of cells over-expressing SisOLD. Cells cultured in the induction medium were taken at different time points and observed under a NIKON-E microscope. Upper, middle, and lower panels, 0, 12, and 24h. Scale bars: 2 μm. (**C**) Cell size statistics of the data in (B). Cell cultures were sampled at the indicated time points and observed under the microscope. The diameters of ~100 cells were measured using ImageJ software for each culture repeat. (**D**) Flow cytometry analysis of the DNA content of Sis/pSeSD and Sis/pSeSD-SisOLD cells cultured in MATV medium.

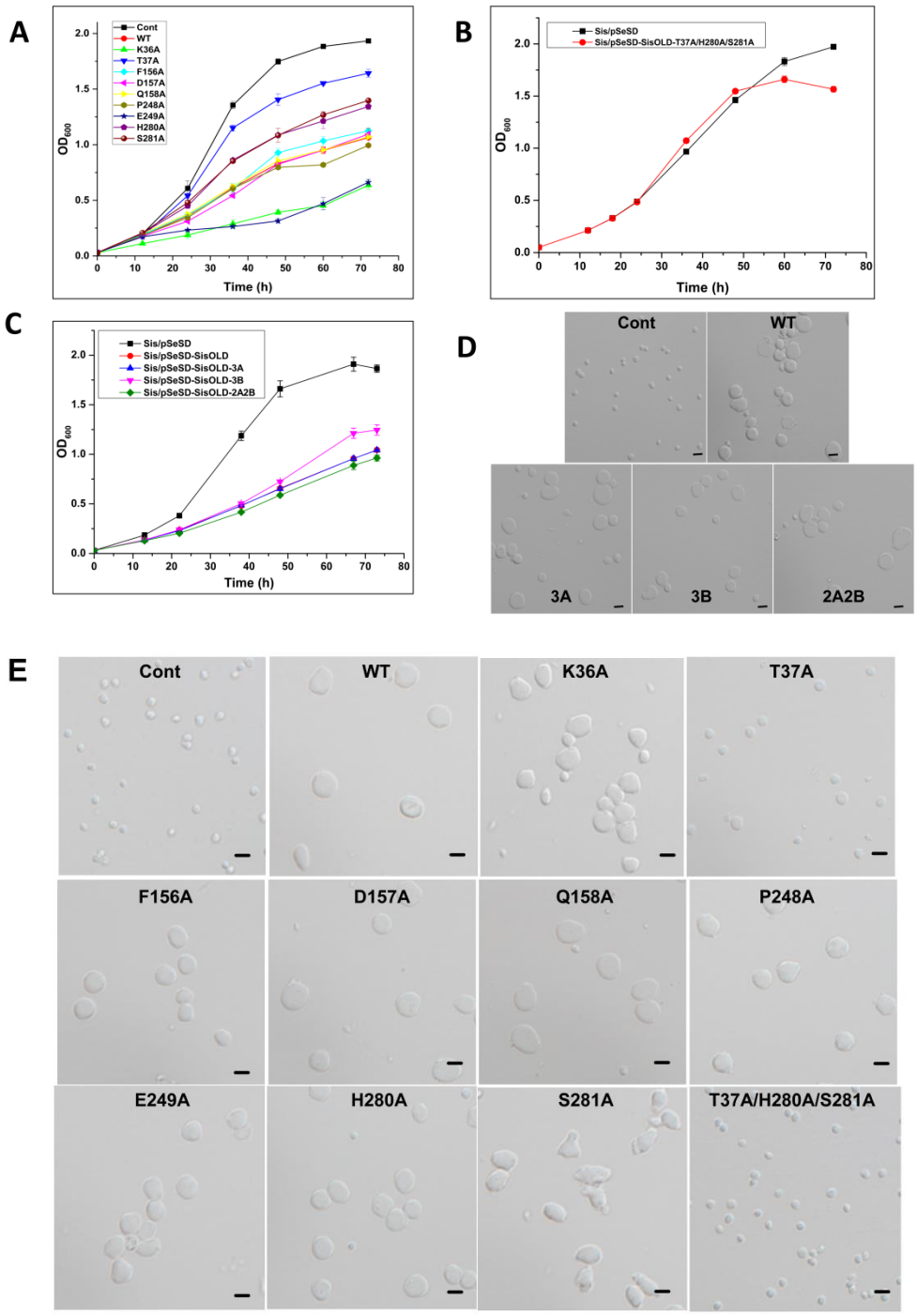

Figure 6. The ATPase activity of SisOLD is vital for cell cycle progression. (**A**) Overexpression growth curve analysis of a single ATPase key amino acid mutant. (**B**) Overexpression growth curve analysis of T37，H280 and S281 combination mutants. (**C**) Growth curves of metal ion binding site mutant overexpression strains. 3A represents the E338A，L391A，D393A combination mutation, 3B represents the

E341A，E409A，E411A combination mutation, and 2A2B represents the L391A，D393A，E409A，E411A combination mutation. (**D**)indicates the cellular morphology of the overexpression strain in (C), taken from a sample induced by arabinose for 24h; Scale bars: 2 μm. (**E**) Cell morphology analysis of overexpression strains in (A) and (B). Samples were taken from arabinose induction for 24h; Scale bars: 2 μm.

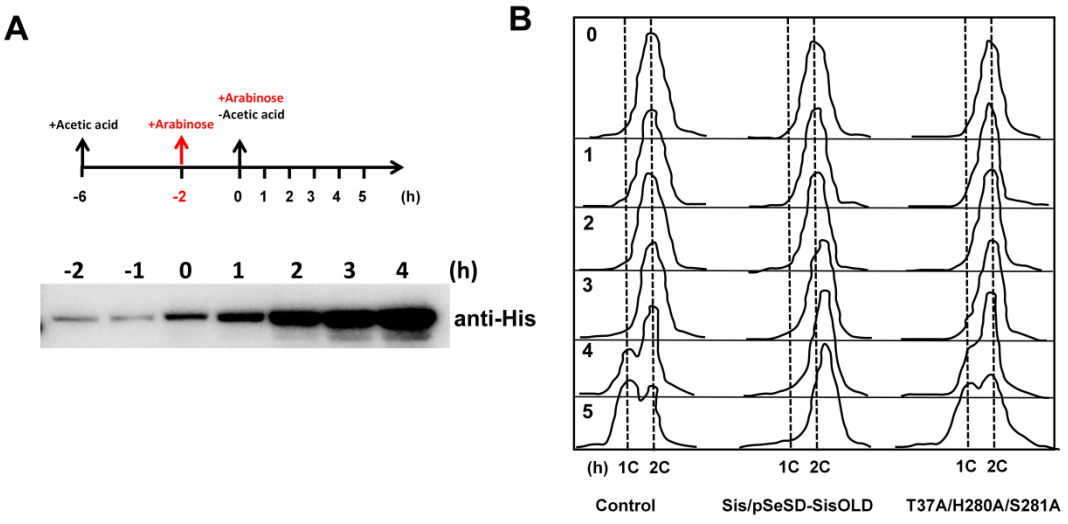

Figure 7. Overexpression of SisOLD blocks the process of cell division. (**A**) A schematic showing cell synchronization and induction of SisOLD over-expression with arabinose (0.2%). The time for the acetic acid treatment and arabinose induction are indicated. E233S containing the empty plasmid (Sis/pSeSD) was used as a control. (**B**) Flow cytometry profiles of DNA content distribution of cells 0-5 hrs after acetic acid removal.

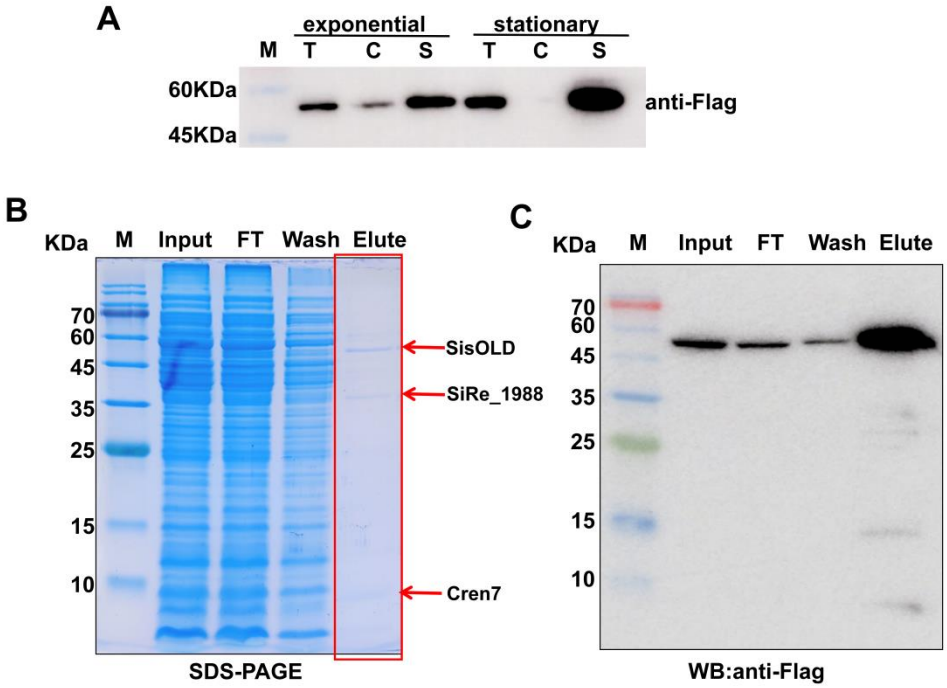

Figure 8. Subcellular localization and analysis of the cellular amount as well as associated proteins. (**A**) Cellular localization of SisOLD in the cytoplasm or chromatin of cells during the exponential phase (OD_{600}=0.4) of cell growth as well as in stationary cells (OD_{600}=1.0). T, total protein. C, Chromatin fractions. S, Soluble fractions. (**B**) SDS-PAGE and (**C**) Western blotting of immunoprecipitation of SisOLD *in-situ* Flag strains. Input represents cell lysate, FT indicates flow-through, Wash indicates washing of magnetic beads using buffer A to remove nonspecifically bound fractions and elute indicates elution fractions of target proteins.